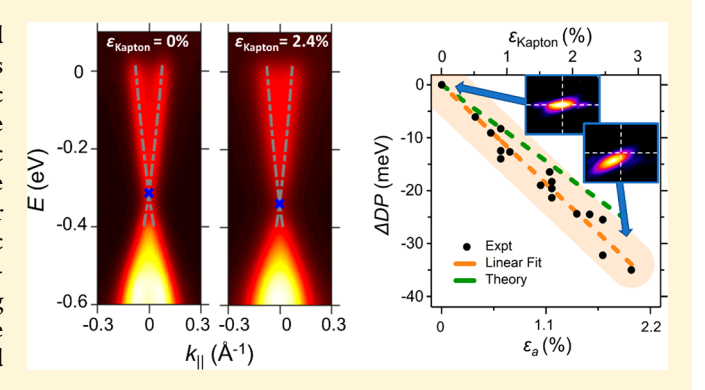
In Situ Strain Tuning of the Dirac Surface States in Bi₂Se₃ Films

David Flötotto,**,†,‡® Yang Bai,†,‡ Yang-Hao Chan,§ Peng Chen,†,‡, Xiaoxiong Wang,¹ Paul Rossi,‡ Cai-Zhi Xu,†,‡ Can Zhang,†,‡ Joseph A. Hlevyack,†,‡ Jonathan D. Denlinger, Hawoong Hong, Mei-Yin Chou,§,○,◆® Eric J. Mittemeijer,‡,↑ James N. Eckstein,†,‡ and Tai-Chang Chiang*,†,‡,

Supporting Information

ABSTRACT: Elastic strain has the potential for a controlled manipulation of the band gap and spin-polarized Dirac states of topological materials, which can lead to pseudomagnetic field effects, helical flat bands, and topological phase transitions. However, practical realization of these exotic phenomena is challenging and yet to be achieved. Here we show that the Dirac surface states of the topological insulator Bi₂Se₃ can be reversibly tuned by an externally applied elastic strain. Performing in situ X-ray diffraction and in situ angleresolved photoemission spectroscopy measurements during tensile testing of epitaxial Bi₂Se₃ films bonded onto a flexible substrate, we demonstrate elastic strains of up to 2.1% and quantify the resulting changes in the topological surface state.



Our study establishes the functional relationship between the lattice and electronic structures of Bi₂Se₃ and, more generally, demonstrates a new route toward momentum-resolved mapping of strain-induced band structure changes.

KEYWORDS: Topological surface state, strain, ARPES, XRD, DFT, in situ tensile testing

B ecause of the inherent coupling of the electronic structure with the crystal lattice, the application of strain offers a promising pathway to modify the electronic structure of materials. As such, the application of an elastic strain not only has the potential to provide an efficient reversible engineering control of the functional properties of materials 1-5 but also permits access to novel emergent phases⁶ as well as exotic physical phenomena arising from strain-induced latticesymmetry breaking.⁷⁻⁹ For topological insulators (TIs)¹⁰ specifically, theoretical studies indicate that the bulk band gap and the spin-polarized Dirac surface states can be tailored by elastic strain, 11-16 thus inspiring hopes to use elastic strain as an in situ equivalent of chemical-composition tuning for the implementation of "straintronic" devices. 14 However, the realization of these phenomena is advantageous from both the fundamental and applications perspectives. The challenges in achieving strain control lie in the difficulty of controllably

applying strain, characterizing the type and magnitude of the induced strain, and simultaneously measuring the resulting changes of the surface electronic band structure. Intrinsic stresses/strains induced by the lattice mismatch to a substrate into typical TI thin-film samples relax within a few layers of film growth due to the weak interlayer bonding, 17 and only low or local strains have been realized. 18-20 Because of these limitations, recent experiments have only probed the (local) density of states in the vicinity of dislocations by scanning tunneling microscopy¹⁸ or strained polycrystalline films through transport measurements, 20 but here it is nearly impossible to experimentally disentangle the effect of strain on the topological surface state from other complicating factors

Received: May 23, 2018 Revised: July 23, 2018 Published: August 15, 2018



[†]Department of Physics, University of Illinois at Urbana-Champaign, Urbana, Illinois 61801, United States

Frederick Seitz Materials Research Laboratory, University of Illinois at Urbana—Champaign, Urbana, Illinois 61801, United States

[§]Institute of Atomic and Molecular Sciences, Academia Sinica, Taipei 10617, Taiwan

Advanced Light Source, Lawrence Berkeley National Laboratory, Berkeley, California 94720, United States

¹College of Science, Nanjing University of Science and Technology, Nanjing 210094, China

^{*}Max Planck Institute for Intelligent Systems, Heisenbergstraße 3, D-70569 Stuttgart, Germany

Advanced Photon Source, Argonne National Laboratory, Argonne, Illinois 60439, United States

OSchool of Physics, Georgia Institute of Technology, Atlanta, Georgia 30332, United States

[◆]Department of Physics, National Taiwan University, Taipei 10617, Taiwan

[^]Institute for Materials Science, University of Stuttgart, Germany

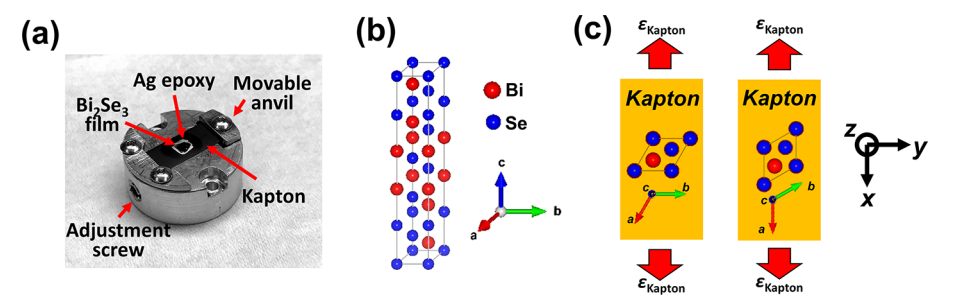


Figure 1. (a) Photo of the strain sample holder. The strain is applied by turning the adjustment screw with a wobble stick, thus moving the anvil and thereby straining the conductive Kapton foil and the attached epitaxial Bi_2Se_3 film. (b) Unit cell of Bi_2Se_3 . (c) Schematic drawings of the Bi_2Se_3 /Kapton samples showing the two choices of orientations of the Bi_2Se_3 films with respect to the direction of elongation of the Kapton foil (indicated by red arrows).

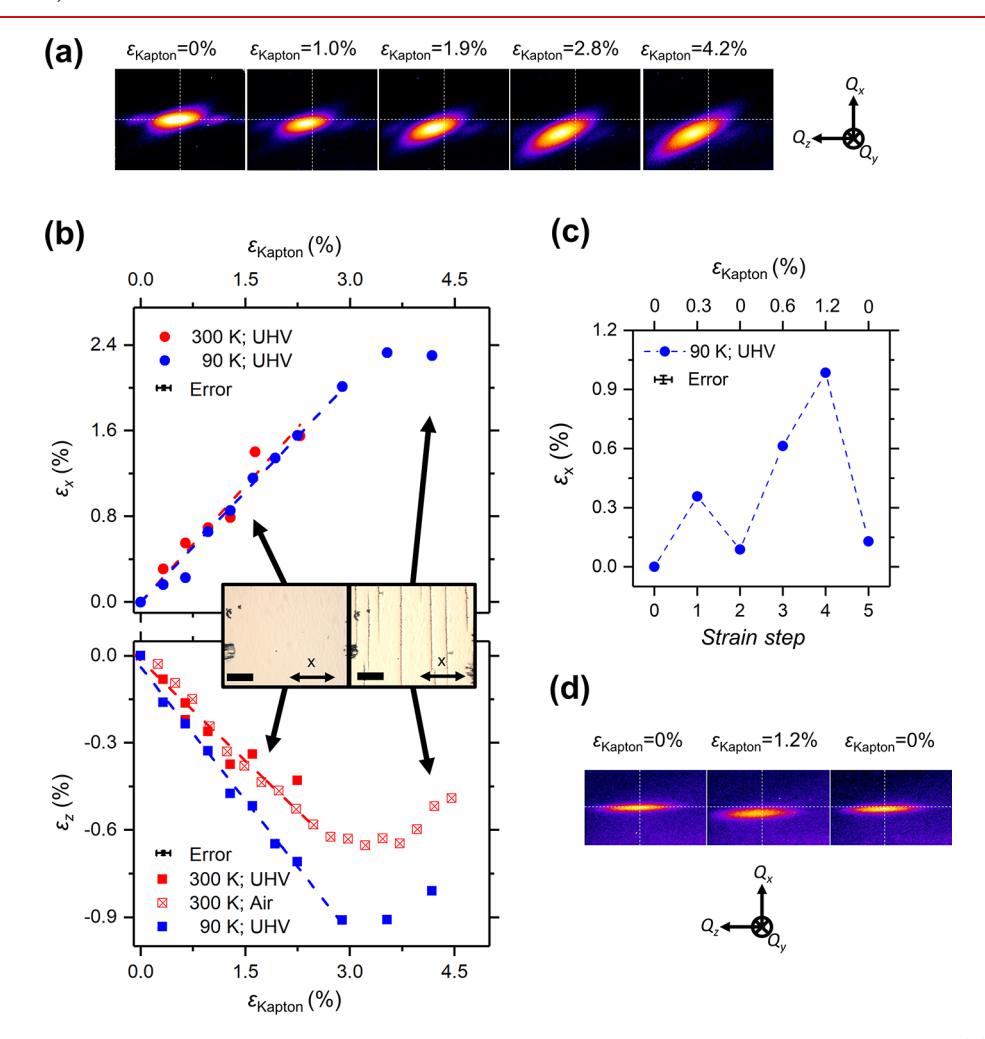


Figure 2. (a) Detector images showing the shift of the 015 reflection for increasing $\varepsilon_{\text{Kapton}}$. The intensity scale is quadratic. (b) Strain components of the Bi₂Se₃ film, ε_x and ε_z as a function of $\varepsilon_{\text{Kapton}}$ under different environments and at different temperatures. The strain in the Bi₂Se₃ films initially increases linearly before it starts to relax by defect formation. The inset presents optical micrographs, demonstrating crack formation at large strains; scale bar 20 μ m. (c) Measured ε_x for cyclic straining and unstraining of the Kapton foil. (d) Detector images showing the reversible shift of the 015 reflection during cyclic straining and unstraining.

such as the presence of electric fields at grain boundaries, ¹⁸ morphological changes, ²¹ and bulk states. ²⁰ Consequently, the direct experimental quantification of the effects of strain on the topological surface state remains elusive.

To advance the application of topological materials in the field of "straintronics", we have developed an approach that enables angle-resolved photoemission spectroscopy (ARPES) and X-ray diffraction (XRD) measurements during tensile

testing of ultrathin epitaxial $\mathrm{Bi}_2\mathrm{Se}_3$ films bonded onto conductive polyimide foils (Kapton). This setup not only allows systematic in situ control of the strain state on a macroscopic length scale but also enables a direct, momentum-resolved quantification of the elastic strain-induced energy shift of the topological Dirac point, which is simply impossible with traditional approaches based on mismatched epitaxial film growth.

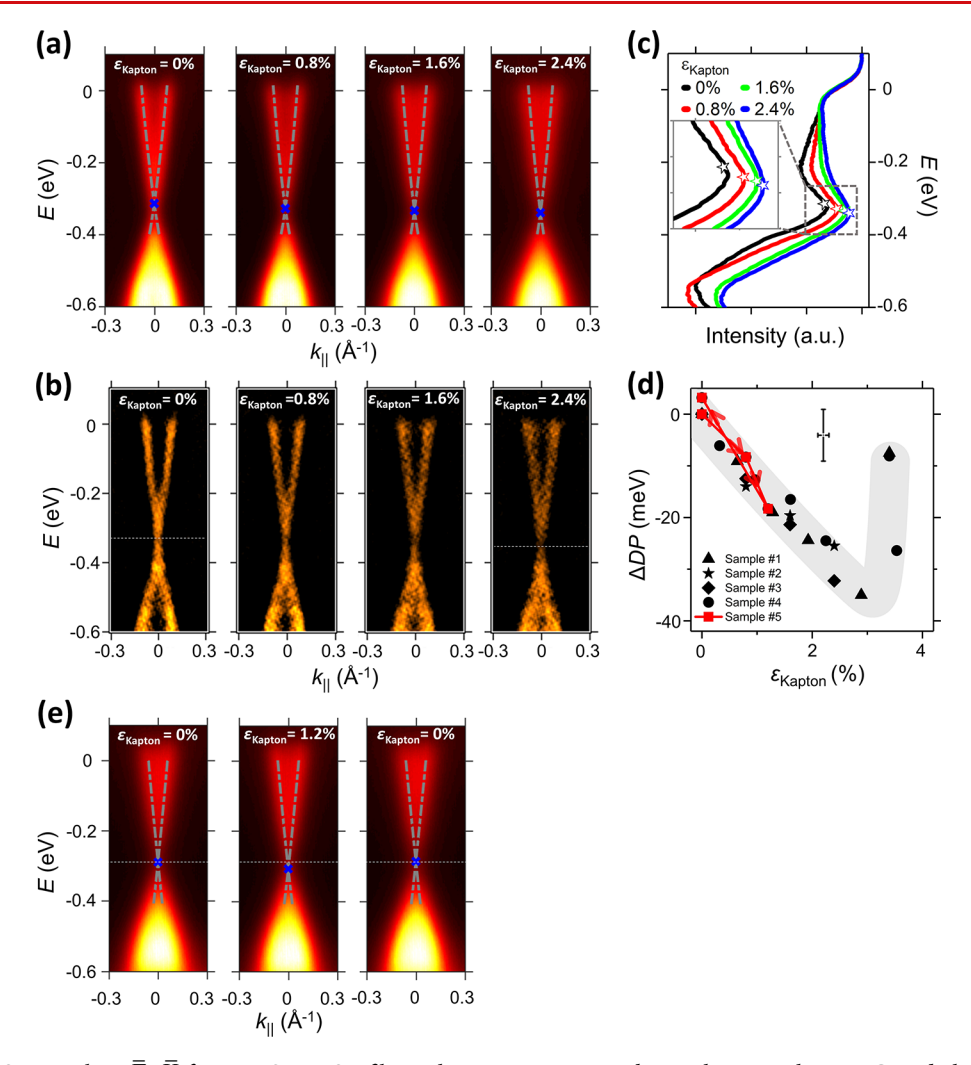


Figure 3. (a) ARPES maps along $\bar{\Gamma} - \bar{K}$ for a 10-QL Bi₂Se₃ film with increasing $\varepsilon_{\rm Kapton}$ taken with 52 eV photons. Gray dashed curves show fitted dispersion relations of the topological surface states, and the blue crosses mark the Dirac points. (b) Corresponding second-derivative ARPES maps. (c) Background-corrected energy dispersion curves at $\bar{\Gamma}$ for various strain levels. Stars mark the Dirac points. (d) Shift of the Dirac point (ΔDP) as a function of $\varepsilon_{\rm Kapton}$ as measured during five independent tensile tests. The red dots are data from a straining/unstraining experiment and the gray line is a guidance to the eyes. (e) ARPES maps along $\bar{\Gamma} - \bar{K}$ during straining/unstraining, demonstrating the elastic nature of the observed Dirac point shifts.

Films of 10- and 12-QL Bi₂Se₃(0001) are epitaxially grown onto thoroughly cleaned Al₂O₃(0001) substrates and capped with a 60 nm thick Nb layer. Each sample ($\sim 3 \times 3 \text{ mm}^2$) was flipped over and glued with the Nb layer downward onto 50 or 125 μ m thick conductive Kapton foils, as extensively used for the fabrication of flexible electronic devices.²² The Al₂O₃/ Bi₂Se₃/Nb/Kapton samples are then mounted on a specially designed strain sample stage for XRD and ARPES measurements to determine the lattice deformation and the band structure of Bi₂Se₃ as a function of the imposed elongation of the Kapton foil. Finally, the Al₂O₃(0001) substrate, providing protection against contamination of the Bi₂Se₃ film, is mechanically cleaved away in situ to expose a fresh Bi₂Se₃ surface. The cleavage occurs exclusively at the Bi₂Se₃/Al₂O₃ interface, leaving the Bi₂Se₃ film with a thickness predetermined by the growth process on the Kapton foil. The experimental setup for accommodating this special "flip-chip" sample assembly and a schematic of the crystallographic orientations of the epitaxial Bi₂Se₃ films are shown in Figure 1.

The strain state of the ultrathin Bi₂Se₃ film was determined by recording reciprocal-space X-ray maps for increasing tensile

strain imposed on the Kapton foil along x, $arepsilon_{ ext{Kapton}}$. Examples of the detector images (Figure 2a) show that, with increasing $\varepsilon_{\text{Kapton}}$, the 015 reflection of Bi₂Se₃ shifts to smaller Q_x and larger Q_z , as a consequence of the imposed expansion of the Bi_2Se_3 lattice along x and the accompanied Poisson contraction along z, respectively. The strain components ε_x and ε_z as a function of $\varepsilon_{\text{Kapton}}$ are summarized in Figure 2b for experiments performed under different environments and at different temperatures. Under all conditions, both ε_x and ε_z initially change linearly with $\varepsilon_{\mathrm{Kapton}}$ and reach maximum values of 2.1 and -0.9%, respectively, for the test conducted at 90 K. The linear behavior up to $\varepsilon_{\rm Kapton} \approx 3\%$ suggests an elastic deformation of the Bi₂Se₃ crystal lattice. Indeed, when the strain applied to the Kapton is released, the reflections essentially shift back to their initial positions (Figure 2c,d), evidencing that enormous macroscopic elastic deformations can be realized in ultrathin $\mathrm{Bi_2Se_3}$ films. For $\varepsilon_{\mathrm{Kapton}}$ exceeding 3%, the strain in the Bi₂Se₃ film does not increase any further, and the reflections broaden significantly, implying the onset of plastic deformation. For even larger $\varepsilon_{\rm Kapton}$ of ~4%, the strain in the Bi₂Se₃ film starts to relax due to the development of

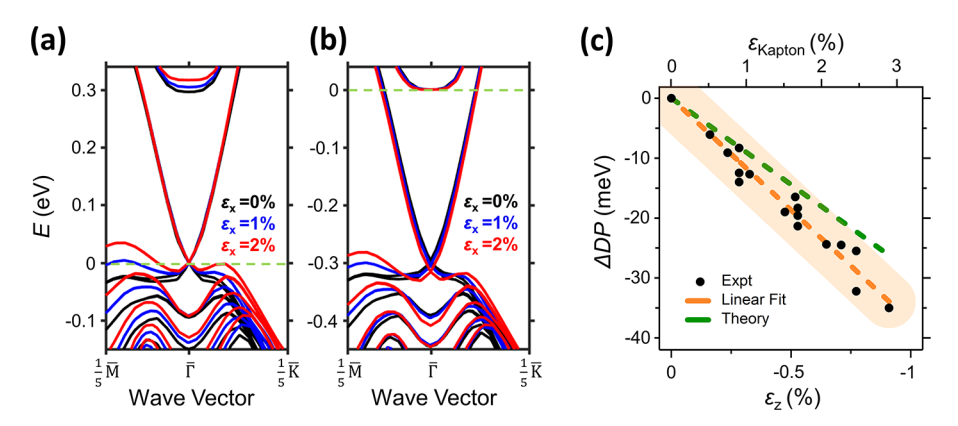


Figure 4. (a) Calculated band structures for a 6-QL ${\rm Bi}_2{\rm Se}_3$ film with the Dirac point set at E=0 for $\varepsilon_x=0$, 1, and 2%, emphasizing the upward shift of the conduction band minimum with increasing strain. (b) Same band structures plotted with the conduction band minimum set at E=0 providing a direct comparison to the electron-doped films in our experiment. (c) Experimental energy shifts (black dots) of the Dirac point relative to the Fermi level (ΔDP) as a function of $\varepsilon_{\rm Kapton}$ and ε_z . The orange dashed line is a linear fit to the data, and the orange shaded area indicates the error margins. Also shown is the theoretical prediction (green dashed line).

cracks, as visible in the optical micrographs (inset in Figure 2b). The slightly larger extent of the linear elastic regime and the enhanced compressive strain along z, ε_z , for the test conducted at low temperatures can be attributed to enhanced van der Waals bonding along the c axis at low temperatures, as reported for the related material Bi₂Te₃. ²³

Figure 3a,b shows ARPES and corresponding secondderivative maps along $\overline{\Gamma} - \overline{K}$ of a Bi₂Se₃ film at various $\varepsilon_{\text{Kapton}}$. The map at $\varepsilon_{\text{Kapton}} = 0\%$ shows the topological surface states with the Dirac point at ~0.34 eV, which is typically observed for $\mathrm{Bi_2Se_3}$ films exhibiting electron doping due to Se vacancies. ²⁴ With increasing $\varepsilon_{\mathrm{Kapton}}$ and the accompanied elastic deformation of the Bi₂Se₃ lattice, the position of the Dirac point moves to lower energies (Figure 3a,b). These shifts are also evident from the energy distribution curves at $\overline{\Gamma}$ (Figure 3c). To quantify the observed shifts, the dispersion relations for the topological surface states are extracted by curve fitting²⁴ (see the Supporting Information), as shown by the dashed curves overlaying the data in Figure 3a. For $\varepsilon_{\mathrm{Kapton}}$ \leq 3%, the Dirac point shifts approximately linearly with $\varepsilon_{\text{Kapton}}$ to lower energies by up to -35 meV (Figure 3d). Within this range of $\varepsilon_{\text{Kapton}}$, where our XRD measurements demonstrated the elastic deformation of the crystal lattice, the Dirac point shifts to lower energies upon straining but returns to the original position upon unstraining (Figure 3d,e). This finding thus indicates the elastic nature of the observed strain-induced band structure changes. For $\varepsilon_{\rm Kapton}$ > 3%, the shift of the Dirac point becomes nonlinear (Figure 3d), in agreement with the relaxation of the film strain revealed by our XRD measurements (cf. Figure 2b).

The experimental results can be directly compared with first-principles calculations for ${\rm Bi}_2{\rm Se}_3$ films subjected to increasing ε_x , where the strain components ε_y and ε_z are given by the Poisson contraction of Kapton and by energy minimization, respectively. These conditions reflect fairly accurately the strain state of the ${\rm Bi}_2{\rm Se}_3$ film during tensile testing, as confirmed by the good agreement of the resulting $\varepsilon_z/\varepsilon_x$ ratio with that determined by XRD at 90 K (-0.41 vs -0.43; cf. Figure 2b). Figure 4a shows the calculated band structure for a 6-QL ${\rm Bi}_2{\rm Se}_3$ film relative to the Dirac point as a function of ε_x . Strain substantially affects the width and energy positions of the valence and conduction bands. For increasing ε_x , the top of the valence band at $\overline{\Gamma}$ remains essentially stationary, which can be

attributed to its strong connection to the Dirac point by analytic continuation of the electronic wave function over a small energy difference. Simultaneously, the increasing compressive strain along z with increasing ε_x enhances the interquintuple-layer coupling of the Se p_z bands, which causes the vertical band gap at $\overline{\Gamma}$ to increase and the conduction band minimum dominated by the antibonding p_z bands of Se to shift upward relative to the Dirac point. 11-13,15,16 However, to provide a direct comparison to the electron-doped films in our experiment with a somewhat populated conduction band (see the Supporting Information), the theoretical results are replotted with the conduction band minimum (or the Fermi level of the doped sample) as the new reference point (Figure 4b). It then follows that the Dirac point shifts to lower energies with increasing ε_r . Our combined XRD and ARPES results directly demonstrate the impact of strain on the position of the Dirac point and, moreover, allow us to quantify the magnitude of the shift to be -37 meV per -1% strain along z, comparable to the theoretical value of -29 meV at equivalent lattice deformations (Figure 4c).

Our demonstrated ability to follow the evolution of the surface electronic structure of a thin film as a function of strain by direct ARPES measurements during tensile testing is crucial for advancing materials design, modification, and control. The potential is enormous, as evidenced by the impact of highpressure research that has opened an entire new field in materials science.²⁵ Our novel approach using a Kapton foil as the strain-transmitting medium in combination with a special flip-chip technique for preparing freshly cleaved surfaces enables us to show that the topological surface states of Bi₂Se₃ can be tuned over an elastic strain range up to $\varepsilon_r \approx$ 2.1%, a level that is simply impossible to achieve in bulk samples due to their much lower yield strength as compared with that of their spatially confined thin-film complements. The approach not only has important implications for the application of topological materials in the field of thin-film straintronics but also opens new routes to systematically explore the role of strain-induced band structure changes for a wide range of fundamental physical phenomena such as superconductivity,^{7,9} charge density wave formation,²⁶ and direct/indirect band-gap transitions.

ASSOCIATED CONTENT

S Supporting Information

The Supporting Information is available free of charge on the ACS Publications website at DOI: 10.1021/acs.nanolett.8b02105.

Additional information about the sample preparation, the experimental setup, the DFT calculations, the fitting of the topological surface state, as well as its stability over time. (PDF)

AUTHOR INFORMATION

Corresponding Authors

*D.F.: E-mail: flototto@illinois.edu.

*T.-C.C.: E-mail: tcchiang@illinois.edu: Tel. (217) 333-2593.

ORCID ®

David Flötotto: 0000-0001-9113-8889 Mei-Yin Chou: 0000-0003-0113-7191

Author Contributions

D.F. and T.-C.C. organized the project. D.F., P.C., C.-Z.X., and J.D.D. performed the ARPES measurements. D.F., Y.B., C.Z., J.A.H, and J.N.E. designed and prepared the samples. D.F., P.R., Y.B., E.J.M., and H.H. performed the XRD measurements. D.F. and T.-C.C. designed the strain sample holder. X.W., Y.-H.C., and M.-Y.C. performed the first-principles calculations. All authors have participated in discussions of the results and contributed to the manuscript. All authors have given approval to the final version of the manuscript.

Notes

The authors declare no competing financial interest.

ACKNOWLEDGMENTS

This research is supported by (i) the U.S. National Science Foundation (Grant No. DMR-17-09945 for T.-C.C. and No. DMR-11-05998 for J.N.E.), (ii) the Deutsche Forschungsgemeinschaft (FL 974/1-1), (iii) the U.S. Department of Energy, Office of Science, Office of Basic Energy Sciences, Division of Materials Science and Engineering (Award No. DE-AC02-07CH11358 for J.N.E.), (iv) the Thematic Project at Academia Sinica (AS-106-TP-A07), (v) the National Natural Science Foundation of China (No. 11204133), and (vi) the Fundamental Research Funds for the Central Universities of China (No. 30917011338). The Advanced Light Source is supported by the Director, Office of Science, Office of Basic Energy Sciences, of the U.S. Department of Energy under Contract No. DE-AC02-05CH11231. Argonne National Laboratory and work performed at the Advanced Photon Source at Argonne National Laboratory was supported by the U.S. Department of Energy (DOE), Basic Energy Sciences, under Contract No. DE-AC02-06CH11357. Part of the work was carried out in the Central Research Facilities of the Frederick Seitz Materials Research Laboratory.

■ REFERENCES

- (1) Li, J.; Shan, Z.; Ma, E. MRS Bull. 2014, 39, 108-114.
- (2) Roldán, R.; Castellanos-Gomez, A.; Cappelluti, E.; Guinea, F. J. Phys.: Condens. Matter 2015, 27, 313201.
- (3) Mavrikakis, M.; Hammer, B.; Nørskov, J. K. *Phys. Rev. Lett.* **1998**, 81, 2819–2822.
- (4) Ando, Y.; Fu, L. Annu. Rev. Condens. Matter Phys. 2015, 6, 361-381.
- (5) Engelmann, J.; Grinenko, V.; Chekhonin, P.; Skrotzki, W.; Efremov, D. V.; Oswald, S.; Iida, K.; Hühne, R.; Hänisch, J.;

Hoffmann, M.; Kurth, F.; Schultz, L.; Holzapfel, B. Nat. Commun. 2013, 4, 2877.

- (6) Feng, Y.; Wang, J.; Palmer, A.; Aguiar, J. A.; Mihaila, B.; Yan, J. Q.; Littlewood, P. B.; Rosenbaum, T. F. Nat. Commun. 2014, 5, 4218.
- (7) Steppke, A.; Zhao, L.; Barber, M. E.; Scaffidi, T.; Jerzembeck, F.; Rosner, H.; Gibbs, A. S.; Maeno, Y.; Simon, S. H.; Mackenzie, A. P.; Hicks, C. W. Science 2017, 355, eaaf9398.
- (8) Tang, E.; Fu, L. Nat. Phys. 2014, 10, 964-969.
- (9) Ruan, J.; Jian, S.-K.; Yao, H.; Zhang, H.; Zhang, S.-C.; Xing, D. Nat. Commun. 2016, 7, 11136.
- (10) Hasan, M. Z.; Kane, C. L. Rev. Mod. Phys. 2010, 82, 3045-3067.
- (11) Young, S. M.; Chowdhury, S.; Walter, E. J.; Mele, E. J.; Kane, C. L.; Rappe, A. M. Phys. Rev. B: Condens. Matter Mater. Phys. 2011, 84, 085106.
- (12) Aramberri, H.; Muñoz, M. C. Phys. Rev. B: Condens. Matter Mater. Phys. 2017, 95, 205422.
- (13) Liu, W.; Peng, X.; Tang, C.; Sun, L.; Zhang, K.; Zhong, J. Phys. Rev. B: Condens. Matter Mater. Phys. 2011, 84, 245105.
- (14) Zhao, L.; Liu, J.; Tang, P.; Duan, W. Appl. Phys. Lett. 2012, 100, 131602.
- (15) Luo, X.; Sullivan, M. B.; Quek, S. Y. Phys. Rev. B: Condens. Matter Mater. Phys. 2012, 86, 184111.
- (16) Liu, J.; Xu, Y.; Wu, J.; Gu, B.-L; Zhang, S. B.; Duan, W. Acta Crystallogr., Sect. C: Struct. Chem. 2014, 70, 118–122.
- (17) Vyshnepolsky, M.; Klein, C.; Klasing, F.; Hanisch-Blicharski, A.; Horn-von Hoegen, M. Appl. Phys. Lett. 2013, 103, 111909.
- (18) Liu, Y.; Li, Y. Y.; Rajput, S.; Gilks, D.; Lari, L.; Galindo, P. L.; Weinert, M.; Lazarov, V. K.; Li, L. Nat. Phys. **2014**, *10*, 294–299.
- (19) Zeljkovic, I.; Walkup, D.; Assaf, B. A.; Scipioni, K. L.; Sankar, R.; Chou, F.; Madhavan, V. *Nat. Nanotechnol.* **2015**, *10*, 849–853.
- (20) Park, S. H.; Chae, J.; Jeong, K. S.; Kim, T.-H.; Choi, H.; Cho, M.-H.; Hwang, I.; Bae, M.-H.; Kang, C. *Nano Lett.* **2015**, *15*, 3820–3826.
- (21) Kim, T.-H.; Jeong, K. S.; Park, B. C.; Choi, H.; Park, S. H.; Jung, S.; Park, J.; Jeong, K.-H.; Kim, J. W.; Kim, J. H.; Cho, M.-H. *Nanoscale* **2016**, *8*, 741–751.
- (22) Akinwande, D.; Petrone, N.; Hone, J. Nat. Commun. 2014, 5, 5678.
- (23) Jenkins, J. O.; Rayne, J. A.; Ure, R. W. Phys. Rev. B 1972, 5, 3171-3184.
- (24) Zhang, Y.; He, K.; Chang, C.-Z.; Song, C.-L.; Wang, L.-L.; Chen, X.; Jia, J.-F.; Fang, Z.; Dai, X.; Shan, W.-Y.; Shen, S.-Q.; Niu, Q.; Qi, X.-L.; Zhang, S.-C.; Ma, X.-C.; Xue, Q.-K. *Nat. Phys.* **2010**, *6*, 584–588.
- (25) Mao, H.-K.; Chen, X.-J.; Ding, Y.; Li, B.; Wang, L. Rev. Mod. Phys. 2018, 90, 015007.
- (26) Gan, L.-Y.; Zhang, L.-H.; Zhang, Q.; Guo, C.-S.; Schwingenschlogl, U.; Zhao, Y. Phys. Chem. Chem. Phys. **2016**, 18, 3080–3085.